Tellus (1995), 47B, 331–352
Printed in Belgium – all rights reserved

TELLUS
ISSN 0280–6509

Eddy correlation measurements of size-dependent cloud droplet turbulent fluxes to complex terrain

By RICHARD J. VONG* and ANDREW S. KOWALSKI, *College of Oceanic and Atmospheric Sciences, Oregon State University, Corvallis, Oregon 97331-2209, USA*

(Manuscript received 21 March 1994; in final form 15 August 1994)

ABSTRACT

An eddy correlation technique was used to measure the turbulent flux of cloud droplets to complex, forested terrain near the coast of Washington State during the spring of 1993. Excellent agreement was achieved for cloud liquid water content measured by two instruments. Substantial downward liquid water fluxes of ~1 mm per 24 h were measured at night during "steady and continuous" cloud events, about twice the magnitude of those measured by Beswick et al. in Scotland. Cloud water chemical fluxes were estimated to represent up to 50% of the chemical deposition associated with precipitation at the site. An observed size-dependence in the turbulent liquid water fluxes suggested that both droplet impaction, which leads to downward fluxes, and phase change processes, which can lead to upward fluxes, consistently are important contributors to the eddy correlation results. The diameter below which phase change processes were important to observed fluxes was shown to depend upon $\sigma_L/\bar{L}$, the relative standard deviation of the liquid water content (LWC) within a 30-min averaging period. The crossover from upward to downward LW flux occurs at 8 μm for steady and continuous cloud events but at ~13 μm for events with a larger degree of LWC variability. This comparison of the two types of cloud events suggested that evaporation was the most likely cause of upward droplet fluxes for the smaller droplets (dia < 13 μm) during cloud with variable LWC ($\sigma_L/\bar{L} > 0.3$).

1. Introduction

For aerosol particles that nucleate during cloud formation (CCN), the associated increase in size as the droplets grow greatly increases the probability of deposition. The direct interception of cloud droplets by vegetation, referred to as "occult deposition" because it is not measured by rain gauges, can be important for coastal and high-elevation forests because of the beneficial effects of the water deposition and the potentially deleterious effects of the solute deposited with the cloudwater. In areas with frequent wind-driven surface cloud, the chemical fluxes that result from droplet interception by vegetation have been estimated as comparable in magnitude to those associated with precipitation (Vong et al., 1991; Lovett and Kinsman, 1990). Most current estimates of cloudwater chemical inputs to forest are based on models that have not been verified by measurements (Mueller, 1991; Miller et al., 1993; Lovett, 1984). In fact, little is known about the rates of the relevant processes and resulting deposition to vegetation.

Quantification of the rate of exchange of mass between the atmosphere and biosphere can be accomplished using micrometeorological, enclosure, or mass balance techniques. The eddy correlation technique is a micrometeorological method that interprets covariances between wind components and a scalar as turbulent fluxes (Wesley, 1983; Dabberdt et al., 1993); the instru-

* Corresponding author.

ment response times must be sufficiently short to resolve the major transporting eddies. Here,

$$F=\frac{1}{N}\sum\{(L-\bar{L})\times(w-\bar{w})\}=\frac{1}{N}\sum(w'L')$$

$$=\overline{(wL)}-\bar{w}\times\bar{L}, \quad (1)$$

where

L' = deviation of scalar L from its mean $\bar{L}$,

w' = deviation of wind component w from its mean $\bar{w}$,

F = turbulent liquid water (LW) flux along the w orientation.

Interpretation of the measured fluxes generally relies on a knowledge of the type and locations of the sources and sinks for the scalar quantity of interest. In most eddy correlation studies a single hypothesized surface sink (deposition) or source is postulated for a conserved scalar; in a cloud the potential exists for multiple sources and sinks of droplets.

In non-precipitating, warm boundary layer clouds, the vertical distribution of cloud droplets is controlled by phase-change processes, transport by gravity and turbulence, and impaction onto surface vegetation. Phase change processes include CCN activation, droplet condensational growth, and droplet evaporation. Entrainment of sub-saturated air can dilute cloud LWC and evaporate droplets (Blyth et al., 1980; Baker et al., 1982). Droplet gravitational settling becomes important for diameters greater than 20 μm where fall speeds exceed 2 cm s^{-1}. In precipitating clouds, gravitational settling and collision-coalescence become increasingly important to the spatial distribution of liquid water content (LWC). Even when consideration is limited to non-precipitating cloud, the relative importance of processes controlling the LWC distribution in a boundary layer cloud is likely to be droplet size and time-scale dependent.

Turbulent fluxes are sometimes described in terms of a mean scaled flux or turbulent deposition velocity (v_{dt}), defined for droplet deposition as the liquid water mass flux divided by the mass concentration of liquid water at 10 m above ground level (agl). Fluxes and liquid water content (LWC) can refer to either values for a given diameter interval or values integrated over the droplet spectrum. By expressing turbulent flux as a mean scaled value for individual droplet sizes, it is easier to detect the dependence of droplet flux on variables other than the droplet size distribution.

This paper reports measurements of size-dependent turbulent fluxes of cloud water from the Cloud and Aerosol Chemistry Experiment (CACHE-1). Liquid water (LW) flux measurements were performed using the eddy correlation technique as a first step towards testing the hypothesis that turbulent deposition to forest is an important sink for cloud droplets in the boundary layer and, thus, confirming recent measurements by a group from the University of Manchester Institute of Science and Technology, UK (Gallagher et al., 1992a, b; Beswick et al., 1991).

2. Experimental

CACHE-1 was conducted from 10 April until 25 May 1993 at the Cheeka Peak Atmospheric Research Station in Washington State. The site is located 4 km from the Pacific Ocean at the summit of a ridge (460 m elevation) that is oriented perpendicular to the SW winds which commonly occur during cloud (Fig. 1). The upwind fetch (17° average slope for 1.25 km) consists of undulating terrain covered by a nearly closed, even-aged canopy of grand fir, typically 6 m in height. Previous chemical sampling (Vong et al., 1988; Covert, 1988) demonstrated that Cheeka Peak receives clean, marine air during the prevailing on-shore flow conditions.

The eddy correlation system consisted of digital and analog hardware and software running on a 80386/387 microcomputer that polled the serial port and on-board data acquisition cards for signals from the fast response instrumentation (winds, liquid water content).

Cloud microphysical measurements consisted of droplet size spectra and droplet concentration, using an aspirated forward scattering spectrometer probe (PMS model FSSP-100: Baumgardner, 1983; Baumgardner et al., 1985), and integrated liquid water content, using an open path, laser-diffraction instrument (GSI model PVM-100; Gerber, 1991). These instruments were deployed at 10 m agl from a rotatable boom extending 3 m upwind of a walk-up sampling tower. The FSSP aspirates droplets through the sample section at 25 m s^{-1}; a tapered inlet (horn) reduces the

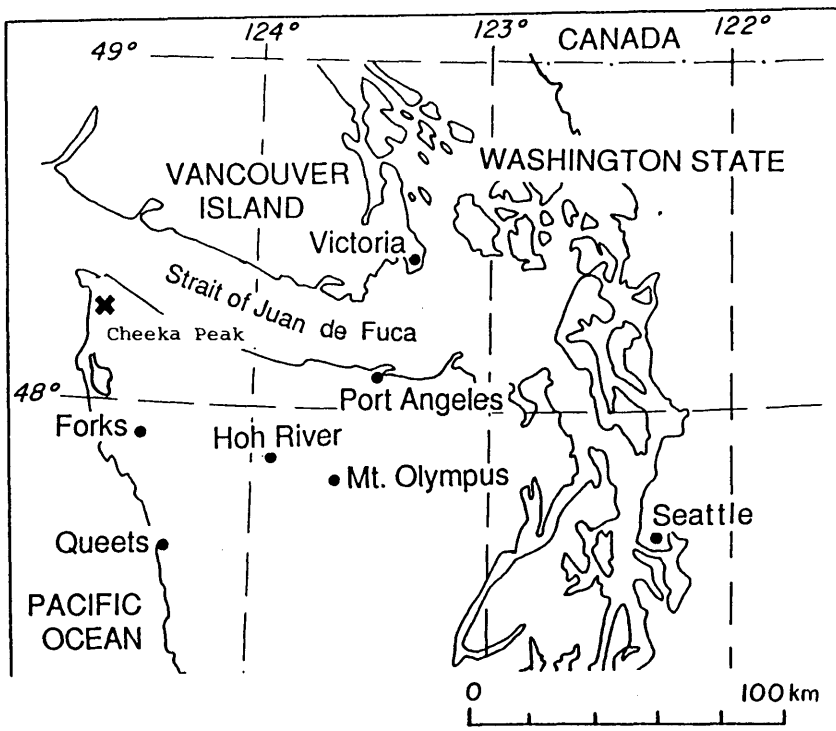

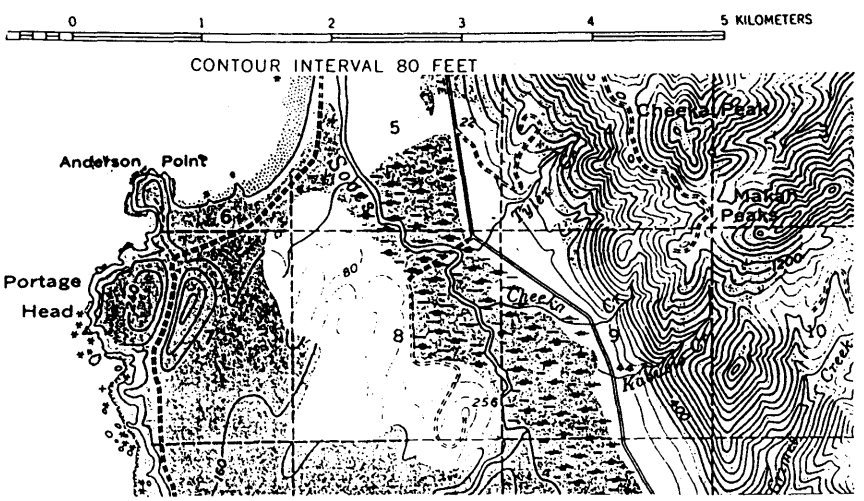

Fig. 1. Map of western Washington State, USA, and the terrain near the Cheeka Peak site.

instrument's face velocity to 8 m s^{-1}. The FSSP and PVM were each oriented at 15° below horizontal (at the mean theta, eq. (3)) and 60 cm cross-wind from a sonic anemometer. Periodic rotations kept the boom-mounted instruments oriented within 10° of the streamwise wind direction to minimize both inlet losses related to large droplet inertia (Norment, 1987; Vincent, 1989) and eddy flux errors associated with sensor flow distortion (Wyngaard, 1988).

The FSSP-100 was optimized for fast operation by increasing its sensing area to 0.738 mm^2 (30% increase in counting rate). The FSSP operation and data access utilized a pulse height analyzer/accumulator (PMS model 1058B) which is software controlled. The PVM-100 was operated at 22 Hz, and its analog output was sampled at 10 Hz by a 12 bit analog-to-digital converter (Intell. Instrument. model PCI 20377W1). The PVM-100 was calibrated periodically using an optical filter. Its offset was tracked by examining the clear-air signal; the instrument's optics were cleaned periodically to keep this baseline in a range corresponding to 0.02 to 0.05 gm/m^3 LWC equivalent. The PVM data were corrected by subtracting this baseline. The FSSP data were converted from number to volume distributions ($2\,\mu m \leqslant dia \leqslant 47\,\mu m$ for 3 μm dia intervals) and integrated LWC using the probe's dynamic sampling volume of 12 cm^3-air/sec and corrections for the probe's electronic deadtime ("activity"). The FSSP size-determination was calibrated using glass beads and confirmed at the University of Washington Cloud and Aerosol Physics Group. No change in the FSSP calibration occurred over the course of CACHE-1.

A sonic anemometer/thermometer (Applied Tech. model SWS-211-3K) provided wind speed along three orthogonal axes, as well as virtual temperature (T_v). The sonic 3-D winds (u, v, and w) were measured at 100 Hz based on transit time differences for forward and reverse sound pulses along each of the 3 axes. T_v was based on the average transit time along the w-axis. The sonic anemometer data were averaged to 10 Hz by the instrument electronics before serial transmission to the logging system. A 2-D analog level sensor and a compass plate tracked the orientation of the boom-mounted instruments.

These "fast system" raw data (most at 10 Hz) were collected simultaneously and continuously, time stamped, logged on the PC hard drive, and backed up to 8-mm tape (Exabyte model 8200) daily for subsequent analyses. Certain derived quantities (e.g., FSSP LWC and droplet concentration, wind direction) were calculated in real time for display and logging. The "fast" system required 180 megabytes of data storage per day.

A second logging system accessed and stored "slower" (1.5 Hz) data as 5-min averages which consisted of wind profiles measured from a second tower (Rohn model 25 g) located 6 m north of the walk-up tower. A twin-propeller commercial anemometer (R. M. Young K-gill, modified with a level sensor) and two single-propeller anemometers (wind monitor; R. M. Young model 05103) measured wind speed from 10 to 12.7 m agl. Vertical and horizontal wind speeds were obtained from the K-gill using the iterative method of Atakturk and Katsaros (1989). All propellers were calibrated in a wind tunnel for linear response and for response to off-axis winds.

In addition to the above measurements, the two logging systems acquired and stored ozone concentration (uv absorbance; Dasibi model 1003 PC), aerosol concentration ($dia \geqslant 10$ nm; TSI model 3760) sampled downstream of a whole air inlet that aspires and evaporates cloud droplets and senses aerosol as the sum of CCN and interstitial aerosol, precipitation rate (tipping bucket gauge), and net radiative flux (REBS, Fritschen). Bulk cloudwater and rainwater chemical compositions were characterized but will be reported elsewhere. Auxiliary meteorological data included surface and 500 mb analyses and 2 × daily rawindsondes (wind, temperature, and T_d profiles) from the National Weather Service (NWS) Quillayute station located 20 km south of Cheeka Peak.

3. Data analysis methodology

3.1. Event selection

The cloud events sampled during CACHE-1 are characterized with regard to how steady and continuous they were. Consistent with analyses by Blyth et al. (1980) and Noonkester (1984), the degree of variability in LWC was selected as an appropriate criteria for defining "steady and continuous cloud". Cloud events with high LWC variability are interpreted to be influenced by subsaturated air entrained from cloud base,

edge, or top. In order that the eddy correlation measurements reflect, as nearly as possible, only a single source or sink of LWC, droplet exchange with the forested surface is evaluated only for the "steady and continuous" cloud cases.

In the present experiment, 5 Hz LWC data from the PVM were averaged over 30 min, and the ratio of the LWC standard deviation to LWC mean was calculated (i.e., $\sigma_L/\bar{L}$); a threshold value of 0.3 for this relative standard deviation was selected for stratifying the data. Based on this "steady and continuous" criteria, 17.5 h ("*a*" events) were selected from ca. 100 hours of non-preciptating cloud events. Since the 0.3 threshold value for $\sigma_L/\bar{L}$ is somewhat arbitrary, cases with $\sigma_L/\bar{L}$ of 0.4 or greater, totalling another 7 h ("*b*" events) of non-precipitating cloud, were analyzed for comparison to the preferred events. Two of the "*b*" event segments consisted of the more variable portions of the same cloud events from which the "*a*" event segments were selected.

3.2. *Coordinate rotations*

Integrated LWC and size-dependent droplet fluxes are determined from the covariance between LWC (either integrated LWC from the PVM or FSSP or the LWC for each FSSP size interval) and the 3 velocity components from the sonic anemometer (eq. (1)). Covariances were calculated for the orthogonal coordinate system corresponding to the sonic anemometer axes and then rotated such that the w and v components of the wind (vertical and transverse, respectively) had zero mean values leaving only one non-zero (streamwise: u) wind component for a particular 30-min period. Rotation criteria follow Wesley (1970) and subsequent applications by McMillen (1986) and Beswick et al. (1991). For rotation through an azimuthal angle of:

$$\eta = \tan^{-1}\frac{\bar{v}}{\bar{u}}, \tag{2}$$

and a vertical (attack) angle of:

$$\theta = \tan^{-1}\frac{\bar{w}}{(\bar{u}^2+\bar{v}^2)^{0.5}} \tag{3}$$

defined over 30-min periods in terms of mean wind components, the correct form of the streamwise-normal component of the scalar flux is given by

$$\overline{w'L'} = \overline{w'L'}_{\text{unrot}}\cos(\theta) - \overline{u'L'}_{\text{unrot}}\sin(\theta)\cos(\eta) - \overline{v'L'}_{\text{unrot}}\sin(\theta)\sin(\eta). \tag{4}$$

A sign convention is adopted where negative streamwise-normal fluxes are towards the surface. Analogous formula for the stress and variances are derived by rotating the individual velocities.

The rotations were quite important for studies at Cheeka Peak because turbulent deposition is evaluated as orthogonal to the mean streamwise wind. This "streamwise-normal" flux is taken to represent a "surface-normal" flux and this distinction is hereafter ignored. No event selection based on wind direction was performed because cloud events occurred with the southerly to westerly winds that encountered the preferred upwind fetch.

3.3. *Spike detection, filtering, and spectra*

The sonic anemometer arms intercept cloud droplets which can, particularly at low windspeeds and high LWC, coalesce and eventually block the instrument's transducers. During the experiment such periods were noted via display monitoring; accumulated water was blotted using Kimwipes, beginning a new sampling period. This tendency of the sonic to serve as a cloudwater collector increased the frequency of data spikes compared to clear air conditions.

For the data presented here, spikes in the sonic anemometer data were identified according to the method of Hojstrup (1993). In this approach, the serial correlation in the data is continually tracked and, based on a calculated memory of the system as well as the most recent observation, the next observation is predicted and that prediction is compared to the measured data value. When the prediction error was unusually large, the measured value is identified as anomalous (a spike). Data spikes were replaced by the predicted value for events with a reasonably small number of spikes ($f \leqslant 1\%$, typically $0.2\% \leqslant f \leqslant 0.3\%$) while other event segments were discarded.

In complex terrain, it becomes increasingly difficult to differentiate between momentum transport by large eddies and the effects of non-stationarity (trends within the 30 min averaging period). During CACHE-1, Reynolds averaged (non-filtered) momentum flux was frequently upward. Following McMillen (1986; 1988), the half-hour data signals were detrended using an

approximation to a running mean (exponential filter) and sensitivity to the filter time constant was examined. The high-pass filtered covariances presented here utilize a time constant of 200 s because that value captured virtually all of the heat and liquid water flux while producing a downward momentum flux for nearly all of the cloud events analyzed.

Friction velocity was calculated from the filtered eddy correlation momentum fluxes as:

$$u^* = (-\overline{u'w'})^{0.5} \tag{5}$$

and from the wind profile logarithmic relationship as:

$$u^* = k\frac{\delta u}{\delta(\ln z)}, \tag{6}$$

where k is the von Karman constant and z represents the streamwise-normal distance to the surface.

Filtering removed data variation over scales much larger than those associated with small scale turbulence in the surface layer, but also eliminated large eddy momentum transport from the eddy correlation results. The second estimates (eq. (6)) of momentum flux (as u^*) were derived from the mean wind profiles and, thus, include the effects of larger eddies.

Fast fourier transforms (FFT) were used to perform spectral decompositions (Blackman and Tukey, 1958) of the unfiltered wind components and LW flux. The spectra were band averaged to 100 degrees of freedom for smoothing. Squared coherence complements spectral density in that coherence allowed determination of a covariance statistical significance in the frequency domain (Jenkins and Watt, 1968).

4. Results

Cloud episodes were frequent during CACHE-1, with the site immersed in cloud during 38% of all hours; one-half of those hours had an hourly average LWC ≥ 0.1 g m^{-3}. These episodes included

Table 1. *Mean liquid water content, droplet size, winds, fluxes, and deposition velocities for two types of cloud events observed at Cheeka Peak during 1993*

Event type	Date	Times (PST)	Cloudwater LWC (g m^{-3})	$\sigma_L/\bar{L}$	vmd (μm)	Winds U	η (°)	θ	LW flux (mg m^{-2} s^{-1})	u^*	Deposition velocity v_{dt}	v_{mt}
"*a*"	4–22	1830–2030	0.42	0.25	18.9	6.4	220	19	4	28	0.95	1.2
	5–01	1851–2151	0.45	0.26	13.2	9.6	270	20	10	52	2.2	2.8
	5–10	1715–2015	0.74	0.24	18.9	3.8	280	16	19	25	2.6	1.6
	5–12	1700–2200	0.37	0.17	12.5	9.1	210	14	9	34	2.4	1.3
	5–21	1945–0142	0.28	0.25	12.8	7.1	220	18	2	24	0.71	0.81
	5–25	1121–1321	0.44	0.17	10.8	4.3	240	7	4	&	0.91	&
"*b*"	4–10	1145–1645	0.15	0.56	11.3	3.8	260	15	#	23	#	1.4
	4–22	1500–1800	0.18	0.58	14.6	7.8	200	16	0	42	0.0	2.3
	5–22	0530–0800	0.25	0.36	14.4	5.4	220	15	1	16	2.0	0.47

& filtered and rotated momentum flux was upward.
# Integrated LW flux was 2 mg m^{-2} s^{-1} upward.
LWC: liquid water content (gm/m^3).
$\sigma_L/\bar{L}$: (standard deviation/mean LWC); dimensionless.
vmd: droplet volume mean diameter (μm).
U: streamwise wind velocity (m/s).
θ: wind attack angle, vertical/horizontal (°).
η: wind direction, horizontal (°).
u^*: friction velocity (cm s^{-1}).
v_{dt}: (turbulent LW flux/LWC); (cm s^{-1}).
v_{mt}: (momentum flux/U); (cm s^{-1}).
"*a*" events: "steady and continuous cloud".
"*b*" events: "variable LWC cloud".

primarily stratocumulus cloud with marine air trajectories; cloud episodes lasted from a few hours to two days. During non-precipitating cloud, mean droplet concentrations normally ranged from 200 to 450 cm^{-3} (maximum = 1000 cm^{-3}) with droplet volume mean diameters (vmd) of 11 to 19 μm, typically 13 μm. Cloud LWC between 0.2 and 0.5 gm m^{-3} was typical of continuous cloudy periods.

Twenty predominantly non-precipitating cloud events from CACHE-1, covering 100 h, were analyzed using the procedures described above. Of these data, portions of 6 events were regarded as steady and continuous cloud ($\sigma_L/\bar{L} \leqslant 0.3$; "*a*" events). Additional cloud data displaying a higher degree of LWC variability ($0.4 \leqslant \sigma_L/\bar{L} \leqslant 0.7$; "*b*" events) were selected for comparison to the "*a*" events. Table 1 presents the mean characteristics for the "*a*" and "*b*" events; notable is the fact that the "*a*" events consistently had higher LWC than the "*b*" events. The "*a*" cloud events are analyzed by examining the temporal progression of the integrated liquid water (LW) flux, the size-dependence of that LW flux, and the time-scale dependence of the LW flux. The "*b*" events, as will be demonstrated, are not particularly suitable for analyzing LW fluxes to the forest canopy but rather are used to help understand the controlling processes.

4.1. Liquid water content

Agreement in the liquid water content (LWC) measured by the FSSP and PVM was excellent. These independent measures of cloud LWC are highly correlated ($r = 0.97$, slope = 1.06) when expressed as 30 minute averages (Fig. 2); correlation extends to the raw 5 Hz LWC ($r = 0.8$) within the 30-min intervals. For one event where the FSSP electronic deadtime ("activity") exceeded 50%, the LWC data for the two instruments disagreed due to coincidence sizing errors. Occasional periods of decreased LWC agreement ($|L_{FSSP} - L_{PVM}|/\bar{L} < 15\%$) displayed no apparent relationship to windspeed, boom alignment, or mean droplet diameter.

Previous investigators have suggested an increase in the FSSP sampling volume, due to wind ramming. This error represents an intermittent, multiplicative factor that has no droplet size dependence. An empirical correction has been suggested for other FSSPs (Choularton et al., 1986; M. Hill, personal communication) relating a sample volume error to the ratio of aspiration and ambient wind velocities as

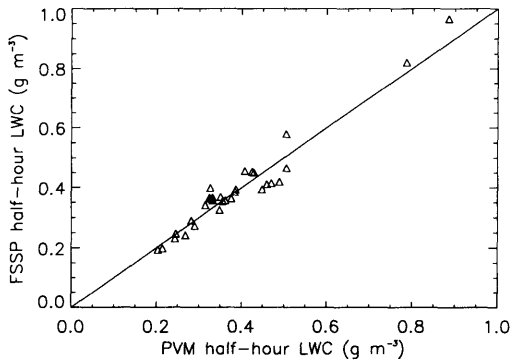

Fig. 2. Cloud liquid water content (LWC) measured by the FSSP versus that from the PVM (30 min averages) during all steady ("*a*") events.

$$\text{ramming} \propto (1 + U_a/U_f), \tag{7}$$

where U_a is the component of the ambient wind down the FSSP throat and U_f is the fan induced velocity in the FSSP's sensing volume. One should obtain anomalously high LWC for the FSSP compared to the PVM if wind ramming alters the FSSP sensing volume.

Values for the FSSP LWC were calculated with and without the wind ramming correction (eq. (7)); the mean LWCs calculated for the PVM and FSSP were often within 4% if no correction was made but differed by 30% (FSSP LWC smaller than PVM LWC) if the correction was applied to the FSSP sensing volume. The correction had minimal effect on the 5 Hz correlation coefficient between FSSP and PVM LWC. Since the two instruments agreed without corrections, no wind ramming correction to mean LWC seems necessary.

Despite the agreement in mean LWC, wind ramming due to gustiness in the horizontal windspeed could be important in the second order FSSP statistics (LW flux and variance). The FSSP consistently produced larger 5 Hz LWC variances than were obtained from the PVM even though the FSSP variance associated with counting statistics generally was small during CACHE-1 (Subsection 4.5).

Fairall (1984) proposed that aspirated, optical particle counting instruments produce streamwise

flux ($u'L'$) errors because the error in sampling volume is correlated to streamwise velocity if wind ramming occurs. The error in streamwise LWC flux is given as

$$\frac{\Delta\overline{u'L'}}{\bar{L}} \propto \overline{u'^2}. \tag{8}$$

Fairall also predicted that a wind ramming error in surface-normal particle flux arises because streamwise and vertical velocities covary (i.e., momentum flux communicates the streamwise LW flux error into the surface-normal LW flux component). The FSSP should overestimate the downward flux of liquid water during wind ramming. Since momentum flux was difficult to measure at the site, the streamwise LW flux represents the most accurate and sensitive indicator of FSSP wind ramming.

The streamwise LW fluxes from the two instruments disagree just as predicted by Fairall (Fig. 3); this is taken as evidence for FSSP wind ramming. Since the PVM (open path design) fluxes are not subject to wind ramming, this result suggests that wind ramming is the largest source of error in the FSSP streamwise liquid water fluxes. The largest disagreements in streamwise and surface-normal LW flux occur during the same events, suggesting that surface-normal FSSP LW fluxes can be overestimated due to wind ramming. Wind ramming corrections were performed by equating surface-normal integrated FSSP LW flux to PVM LW flux; these corrections were applied only to mean-scaled LW flux (deposition velocity) from the FSSP. No LW fluxes or LWC data were corrected. The wind ramming correction involves no change in the size dependence of deposition velocity but does reduce the event-to-event variation in deposition velocity (notably for 1 May).

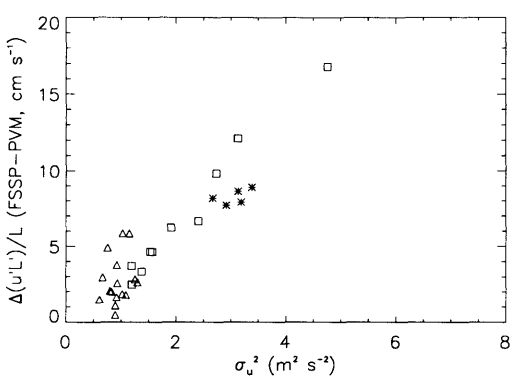

Fig. 3. Comparison of streamwise liquid water flux errors ($\Delta(u'L'/\bar{L})$) with gustiness (streamwise wind variance, σ_U^2) during "*a*" events ($r^2 = 0.85$). Note that the triangles represent the majority of the data; 1 May (asterisks) and 12 May (squares) data display the largest wind ramming errors.

4.2. *Winds; Momentum and heat fluxes*

Similar mean u and w wind velocities and attack angles (theta) were obtained from the propeller and sonic anemometers. The (FFT) spectral shapes for the sonic u, v, and w turbulent wind components (Fig. 4) are consistent with previous findings of an intertial subrange ($-2/3$ slope) at the high frequency end, and suppression of energy in the surface-normal component for the larger eddies (no large-scale components to or from the surface) (Lumley and Panofsky, 1964).

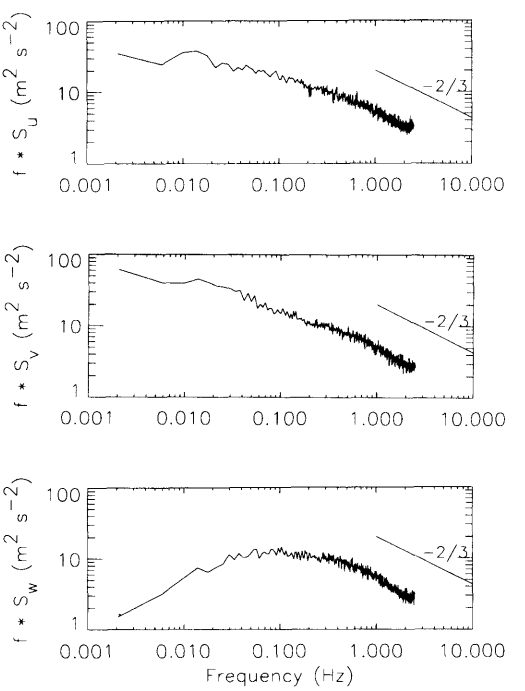

Fig. 4. Spectral estimates for wind components (S_U, S_V, and S_W are the FFT spectral densities for the streamwise, transverse, and surface-normal winds, respectively) which were rotated based on 3.5-h averages for 12 May 1993. Spectral density was multiplied by frequency to preserve the area-variance relationship.

Nearly logarithmic windspeed profiles often were observed; from these profiles friction velocity was calculated for each 30 min averaging period and compared to friction velocity from the eddy correlation measurements for the same period. The profiles suggested a value of 35 cm for the roughness length (Stull, 1988) for this grand fir canopy.

Fig. 5 indicates that the eddy correlation method produced a smaller (by nearly two-thirds) estimate of friction velocity (u^*) than was obtained from the profile method but that the two values were correlated ($r = 0.8$). While the filter appears to remove the effects of non-stationarity from the eddy correlation values for u^* (consistently resulting in the expected downward momentum flux), it apparently removes the downward momentum transport by large eddies. Since the forest canopy is certainly a sink for momentum in the mean

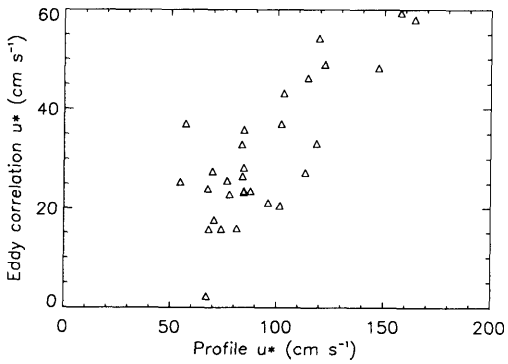

Fig. 5. Friction velocity (u^*) comparison: eddy correlation (eq. (5)) values versus u^* calculated from the wind profile (eq. (6)). The eddy correlation values are smaller because "large eddies" were removed by the filtering technique ($r^2 = 0.61$, slope = 0.38; see text).

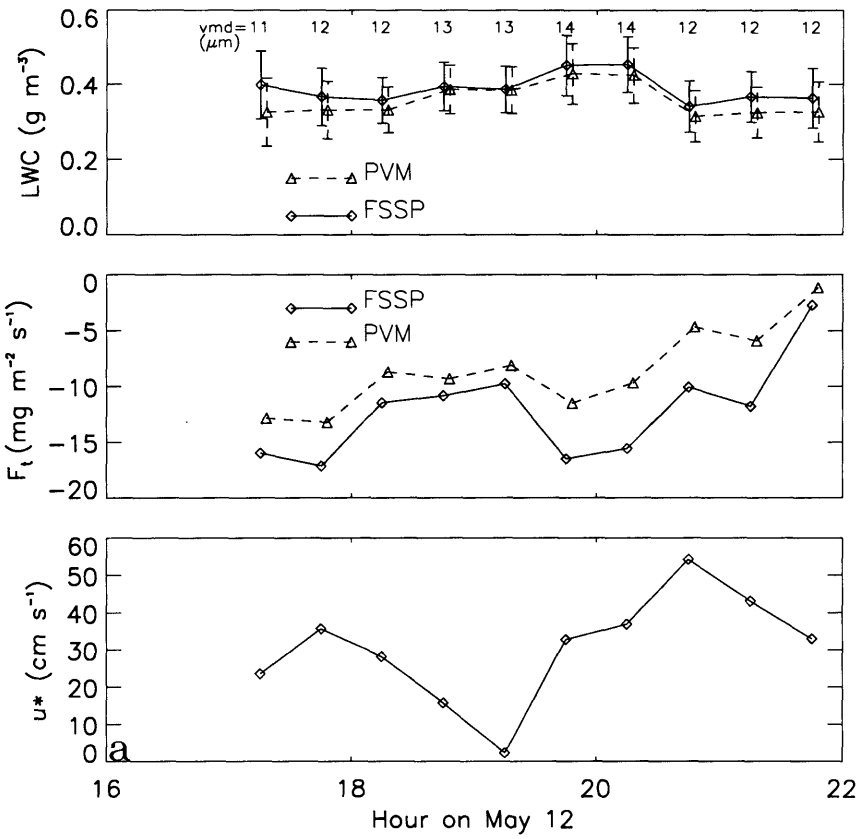

Fig. 6. Time evolution of LWC, uncorrected LW flux (F_{dt}), and friction velocity (u^*) from the eddy correlation measurements for 12 May (panel a: note the wind ramming error as disagreement in LW flux) and 21 May (panel b: note the good agreement in LW flux). Times are plotted at the midpoint of the 30 minute averaging periods.

wind direction, the filtered momentum fluxes (downward) are considered more physically realistic than the unfiltered (upward) momentum fluxes although occasional upward momentum fluxes have been reported, even over relatively flat terrain (Duan et al., 1988).

The eddy correlation heat fluxes suggest that cloud events occurred with nearly neutral stability in that $|R_{if}| < 0.1$, where: R_{if} = flux Richardson number (Stull, 1988). A change in the direction of the heat flux (from small and upward to small and downward) consistently was observed as incoming radiative flux vanished at sunset. The timing of this change in sign of the heat flux generally corresponded to a progression towards the "steady" cloud conditions referred to as "*a*" events here.

4.3. *Liquid water flux: case studies*

Downward integrated LW fluxes consistently were observed during "*a*" events and sometimes were observed during the more variable "*b*" events. Fig. 6 displays both the PVM and FSSP LWC, LW fluxes, and the momentum flux (as u^*) for the two longest "steady", non-precipitating cloud events from CACHE-1: 12 May and 21 May. For both events the PVM and FSSP integrated LW fluxes (F_{dt}) were ~ 1 mm/24 h (11.6 mg m^{-2} s^{-1}). The droplet turbulent fluxes on 12 May were 10–15 mg m^{-2} s^{-1} while those from 21 May were smaller at 1–5 mg m^{-2} s^{-1}. While wind ramming sometimes caused the FSSP to overestimate the downward LW flux, the correlation between FSSP and PVM fluxes that is evident in Fig. 6 suggests that the measured temporal variation in LW flux is real; measurements covarying with LW flux represent possible controlling factors for droplet deposition.

On 12 May, a marine stratus cloud deck moved onto Cheeka Peak at 1600 local time (PST). NWS Quillayute soundings taken at 1600 indicate a

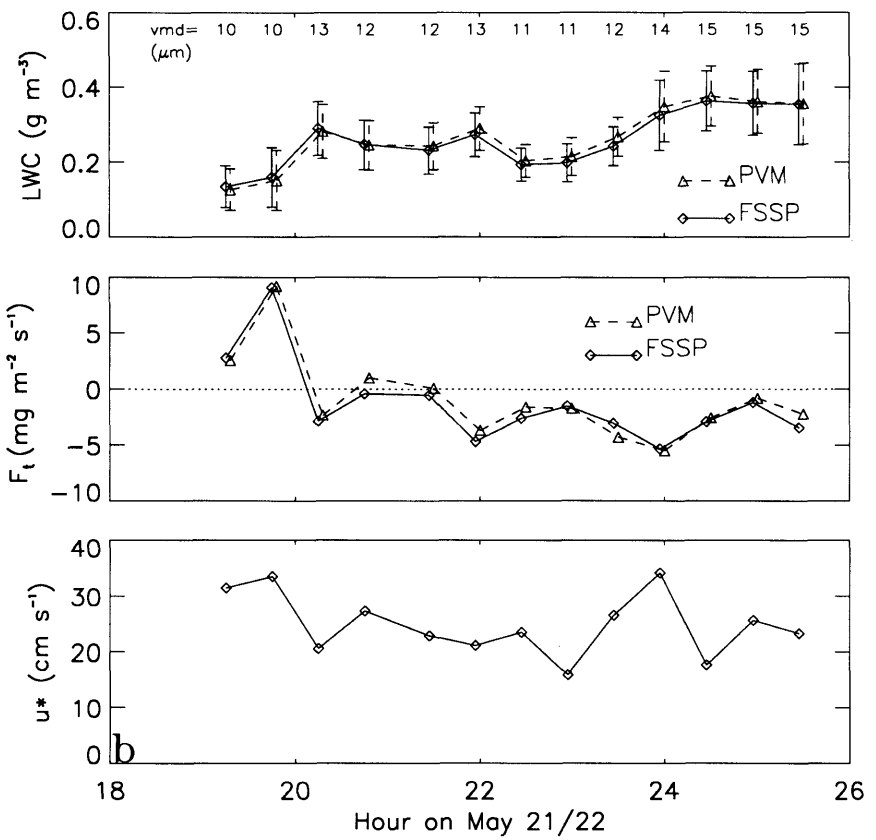

Fig. 6. (cont'd).

strong marine inversion below 850 mb with saturated air below. By 1715 the cloud had thickened and met the "steady and continuous" criterion; during the next 3.5 hours the droplet volume mean diameter (vmd) and LWC increased while both aerosol and droplet number concentrations decreased. As demonstrated in Fig. 6, from 1715 until 2015 changes in integrated LW flux follow changes in friction velocity (except @ 1915 when u^* is suspect). The marked increase in u^* between 1945 and 2045 reflects an increase in windspeed from 8 to 10 m/s. LW flux closely tracks cloud LWC between 1915 and 2045. After 2100 hrs, a marked decrease in LW turbulent flux occurred with the onset of drizzle.

On 21 May, a stratocumulus cloud deck moved onshore during the afternoon bringing thin cloud with occasional precipitation to Cheeka Peak. After 1600 the site was near cloud base and intermittently in cloud. The NWS sounding indicated saturated neutral stability below 800 mb. At 1930 the cloud began to thicken but upward integrated LW fluxes were observed (Fig. 6) until 2000 when droplet volume mean diameter (vmd) increased from 9 to 12 μm and the cloud met the "steady and continuous" ("*a*") criterion. The LW flux usually

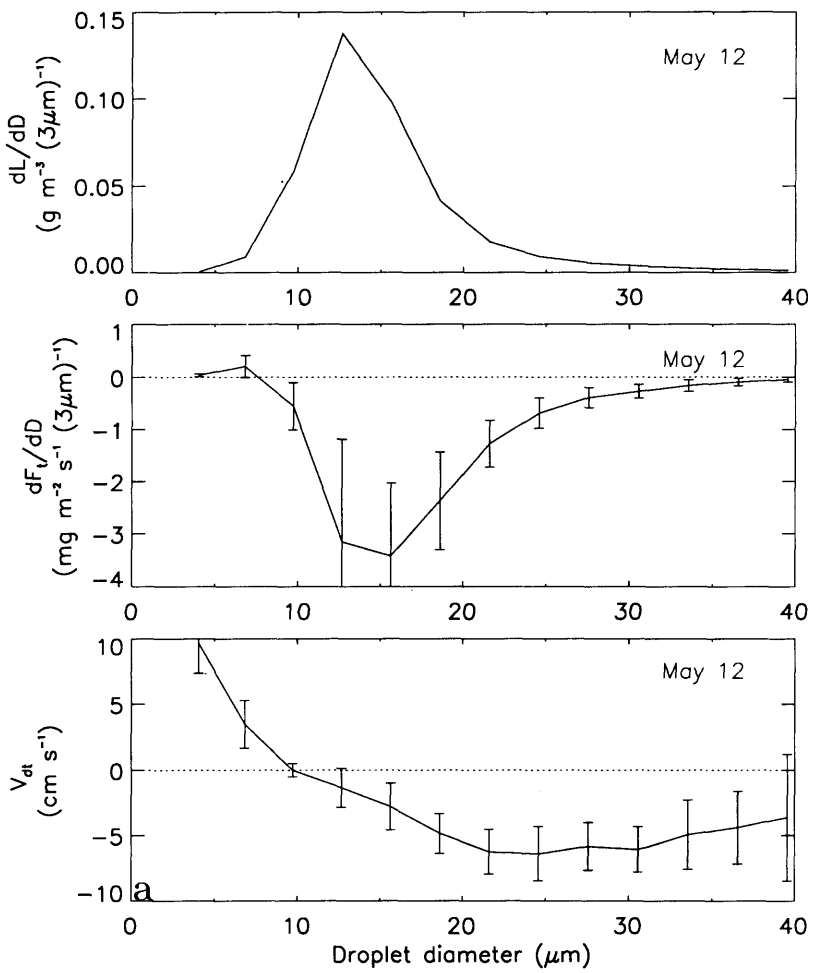

Fig. 7. Size dependence of LWC, LW flux (F_{dt}: 3 μm dia resolution), and deposition velocity (V_{dt}: mean scaled FSSP LW flux. Only the V_{dt} values were wind ramming corrected, see Subsection 4.1) for 12 May (panel a) and 21 May (panel b). Ranges plotted at each diameter represent ± 1 standard deviation about the event mean for 30-min values.

tracked both the friction velocity (except at 2200 for unknown reasons) and the integrated LWC until 2400 when droplet flux decreased as an intermittent and very light drizzle began. The event ended with the occurrence of steady precipitation at 0130 on 22 May.

Additional periods of steady and continuous cloud occurred at Cheeka Peak on 22 April, 1 May, 10 May, and 25 May; all but the last of these event segments represents noctural stratocumulus (Table 1). Notable are 1 May, when Cheeka Peak experienced both high windspeeds and LWC for three hours during which LW fluxes decreased from ~ 20 to 10 mg m^{-2} s^{-1} while friction velocity decreased from 60 to 50 cm s^{-1} and 25 May, when LW fluxes of up to 8 mg m^{-2} s^{-1} occurred during daytime. This last event also differed from the other "*a*" events in that heat flux was upward and unusually high aerosol and droplet concentrations (both ~ 1000 cm^{-3}) were observed.

4.4. *Size-dependent LW flux*

Fig. 7 presents incremental LWC and LW flux (per 3 μm dia interval) as well as mean-scaled LW flux (i.e., deposition velocity) as a function of droplet diameter for two steady and continuous cloud ("*a*") events. These eddy correlation-based values describe only a turbulent component of the LW flux and, thus, represent additions to fluxes that correspond to the mean winds. The size dependence of droplet flux follows the LWC spectra, in that large fluxes occur only at

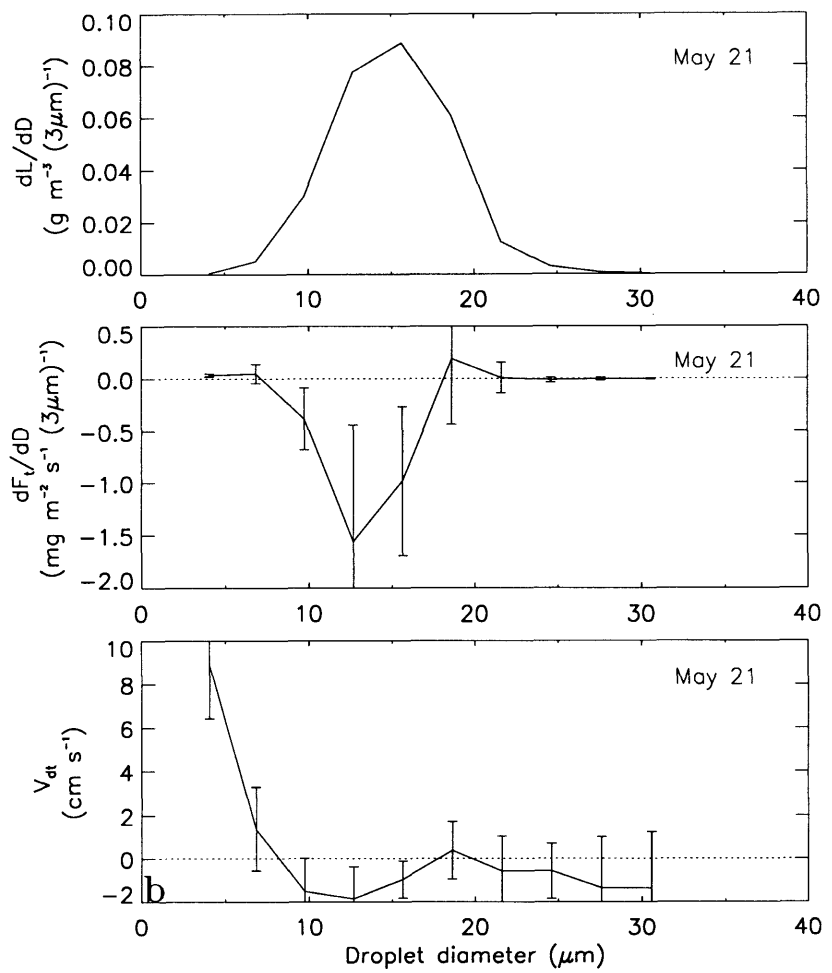

Fig. 7. (cont'd).

droplet diameters with substantial LWC (LWC $\geqslant$ 0.02 gm/m^3/3 μm interval) and maximum flux generally occurs at the same diameter as maximum LWC. For all events the LW flux tends towards small values (or zero) at the same maximum and mininum droplet diameters that LWC vanishes.

For most of the steady and continuous cloud ("*a*") events the turbulent droplet flux at average and large diameters is downward, as depicted for 12 May in Fig. 6. The only upward fluxes for "large" droplets (dia $\geqslant$ 15 μm) were observed for the 22 April and 21 May events for only a single FSSP size interval on each date; these upward fluxes are not significant (relative to within event variability).

Fig. 8 presents droplet number spectra for updrafts ($w' > 0$) and downdrafts from 4 selected "*a*" events. Higher concentrations of small droplets were observed in updrafts while more large droplets were observed in downdrafts; these spectra support the conclusions reached from covariance-based LW fluxes in that upward fluxes of small droplets occur simultaneously with downward fluxes of large droplets. It should be noted that these "conditional" number spectra represent a weaker indication of the turbulent flux than does a covariance because the spectra do not weight droplet concentration by the magnitude of the velocity fluxuations. Nevertheless, these spectra support the observation of a change in the sign of the turbulent LW flux at intermediate droplet diameters.

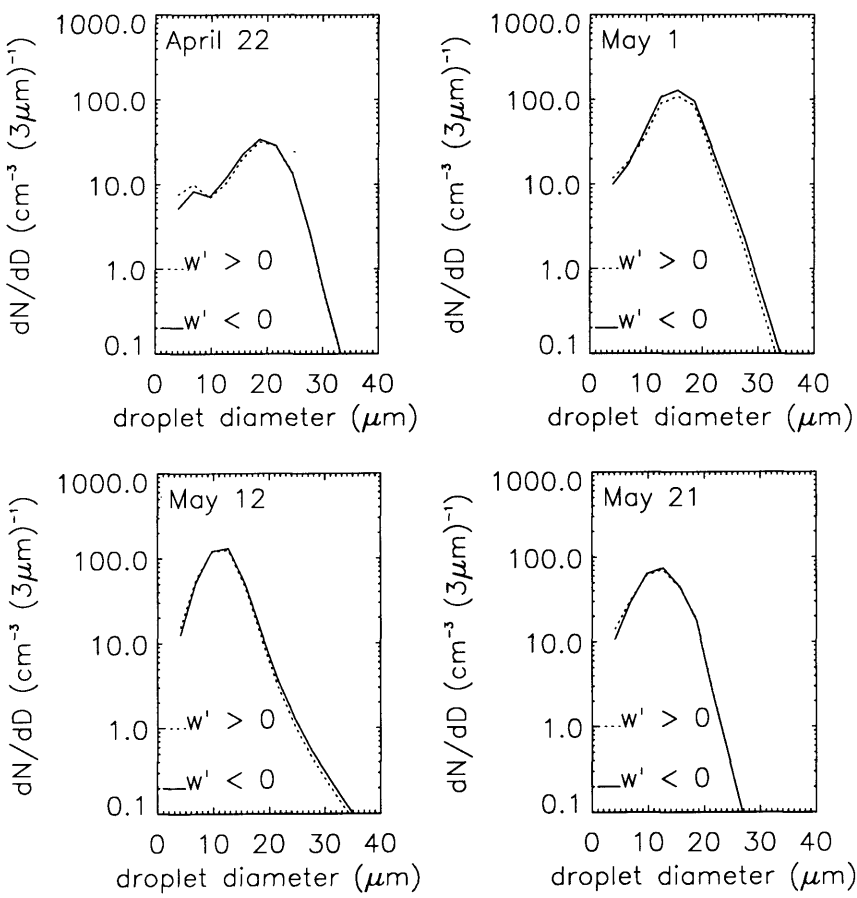

Fig. 8. Average droplet number spectra for updrafts ($w' > 0$; dashed lines) versus downdrafts during four steady cloud ("*a*") events.

4.5. Size-dependent v_{dt}

Measured liquid water (LW) fluxes are presented in Fig. 9 for the "*a*" cloud events as a mean scaled value ($\overline{w'L'}/\bar{L}$, i.e., "deposition velocity", v_{dt}). A consistent size-dependence in scaled LW flux existed for the steady cloud event segments from CACHE-1. In the 10 to 25 μm diameter range, deposition velocities (v_{dt}) were nearly independent of size and typically between 2 and 5 cm/s depending upon event. These deposition velocities for diameters of 10 to 25 μm were significant (most were different than zero based on the within-event variability). At large diameters the errors in the measured flux become increasing important due to poor Poisson counting statistics (Fairall, 1984; Katen and Hubbe, 1985). Expressed as a deposition velocity, typical FSSP counting errors during CACHE-1 were ± 0.06 cm/s at 19 μm diameter and ± 0.5 cm/s at 34 μm.

A previously unidentified size-dependence in the droplet deposition velocity occurs for droplet diameters less than 8 μm (first two FSSP size bins) in that positive (upward) deposition velocities of 2 to 10 cm/s were measured. This upward flux is a quite robust result for the CACHE-1 "*a*" event segments. The 1 May cloud event segment, while displaying the same spectral shape in v_{dt} as the other events, was shifted towards downward fluxes (this event had the largest wind ramming errors). As noted in the previous section, very little LW flux is associated with these small droplets but the fluxes are consistently upward, suggesting processes other than interception by the forest canopy are controlling the distribution of the smallest droplets during the "*a*" events.

4.6. Dependence of V_{dt} on LWC variability

A comparison of two types of cloud events provides information on how the size-dependence changes as an event departs from the "steady and continuous" ideal case. The steady and continuous ("*a*") events generally were nocturnal while "*b*" events typically describe daytime cloud at Cheeka Peak. The "*a*" events had higher LWC and larger vmd than did the "*b*" events (Table 1). Both types of cloud events occurred with similar wind directions (200–285°), attack angles (usually 14–20° below horizontal), and velocities (4–10 m/s).

Figs. 9 and 11 contrast the size-dependence in droplet deposition velocity for the "*a*" events to that for the "*b*" events (see Table 1 for mean characteristics). The "*b*" events had upward

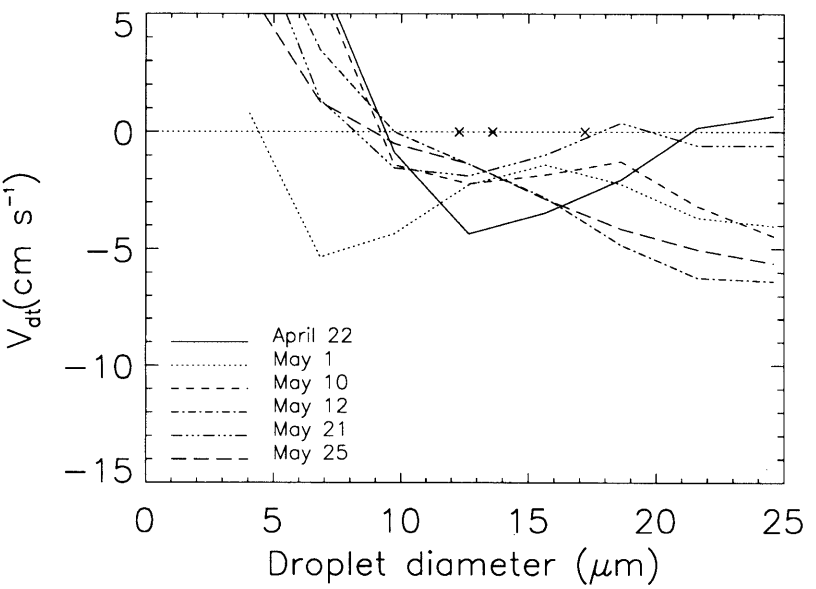

Fig. 9. Mean-scaled liquid water flux, i.e., deposition velocity, v_{dt}, as a function of droplet diameter for 6 steady cloud ("*a*") events. In addition, the crossover points ($v_{dt} = 0$) from upward to downward deposition velocity are plotted for the three "*b*" events (indicated by *X*) for comparison with entire curves for the "*a*" events (see Subsection 4.6).

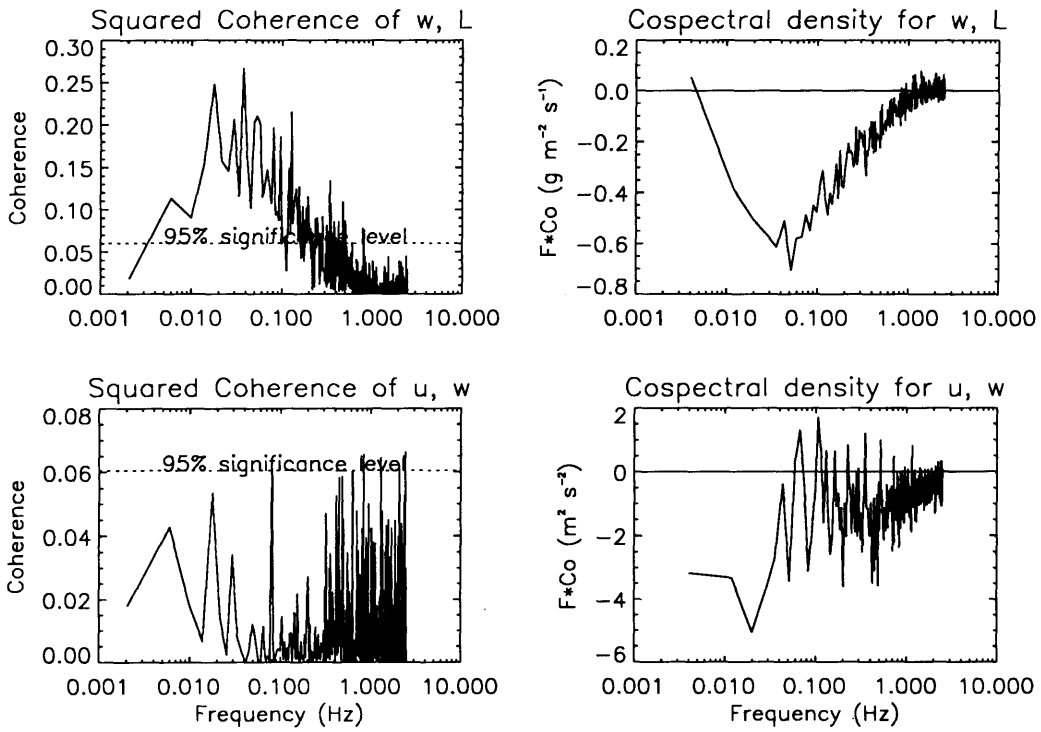

Fig. 10. Cospectral density (frequency decomposition of covariance) and squared coherence (see Subsection 3.3) for vertical motion and liquid water (LW flux) and cospectral information for vertical and horizontal motion (stress or momentum flux). Cospectral density was multiplied by frequency to preserve the area-covariance relationship.

deposition velocities for diameters less than 13 μm but downward for droplet diameters greater than approximately 13 μm. The crossover from upward to downward turbulent LW flux occurs at 8 μm for steady and continuous cloud ("*a*") events.

4.7. Flux time scale

Fig. 10 demonstrates significant covariation (squared coherence: 95% confidence) from 0.006 Hz to 0.3 Hz in the components of surface-normal liquid water flux with an alternate presentation, cospectral density, indicating a downward flux extending to 1 Hz. This is consistent with the fact that the 200 second filter had little effect on the LW flux. Phase spectra (not shown) indicate no out-of-phase covariation in LWC and surface-normal winds. Eddies recurring on ~20 second cyclic time scales transport liquid water at Cheeka Peak based on Fig. 10; thus, a droplet spends approximately 10 s in upward (or downward) moving air before being redirected by the turbulent eddies. An alternate calculation of the turbulent time scale as H/σ_w, where H is the measurement height and σ_w is the standard deviation of the surface-normal wind component, produces time scales of 15–20 s for the "*a*" events. In contrast, the unfiltered momentum flux (Fig. 10) is dominated by longer time scales and, thus, involves larger eddies than were important to LW transport.

5. Discussion

A consistent feature of cloud at Cheeka Peak during CACHE-1 is the occurrence of downward integrated LW turbulent fluxes preferentially during periods of low relative LWC variability ($\sigma_L/\bar{L} < 0.3$) and high LWC. Most of these "*a*" events occurred during the evening. Observations of marine stratocumulus off California also report higher LWC during the evening than during daytime (Betts, 1989; Blaskovic et al., 1991). In

Tellus B/47/3-6

those studies cloud base descends near sundown. During CACHE-1, the increase in droplet size (vmd; Fig. 6) with time leading into "*a*" events suggests that this "steady and continuous" cloud represents observations taken well above cloud base. These "*a*" events contain about twice the LWC relative variability (when calculated on the 0.5 hz basis used by Blyth et al., 1980) as was reported for "adiabatic cloud" above moorland at Great Dun Fell, UK.

Data for non-precipitating cloud were selected for these analyses. Very light drizzle (defined subjectively) was treated as precipitation and, therefore, excluded (except a few short periods). During drizzle, increased droplet sedimentation would reduce the turbulent component of the vertical LW flux of large cloud droplets via erosion of the vertical gradient.

The size distribution of the downward LW fluxes reflects the size distribution of LWC. The downward turbulent fluxes for droplet diameters greater than some critical size (8 to 13 μm depending upon event type) are interpreted to represent a depletion of large droplet concentration at the surface associated with interception by the forest canopy. The measured turbulent LW fluxes are similiar in magnitude (0.3 to 2 mm per 24 h for CACHE-1) to published values obtained over forest and grass using micrometeorological methods (Beswick et al., 1991; Gallagher et al., 1992a, b; Dollard et al., 1983) but smaller than LW turbulent fluxes to forest estimated by models (Mueller, 1991; Miller et al., 1993; Lovett, 1984). Slinn (1982) predicted particle deposition velocities quite similar to CACHE-1 values ("*a*" events: mean $v_{dt} = 3$ cm s^{-1} at dia = 13 μm).

Ordinarily eddy correlation measurements are made over flat, homogeneous terrain, so that the fluxes, which are exact for the point of measurement, can be interpreted as representative of the terrain. In the present study, eddy correlation is used to measure cloud droplet turbulent fluxes to a forest canopy located in complex terrain; the terrain upwind of Cheeka Peak is comparable to two sites where eddy correlation flux measurements have been made recently (Lee et al., 1993; Gallagher et al., 1992b). Inhomogeneous terrain can produce non-equilibrium boundary layers and spatially varying fluxes. The present LW fluxes probably should be regarded as point measurements until their degree of representativeness is determined via simultaneous measurements at several points.

The uncertainties associated with the scalar measurements were small during CACHE-1. LW flux was more sensitive to FSSP wind ramming than was mean LWC although most of the uncorrected FSSP and PVM LW fluxes agreed within $\pm 30\%$, or better (e.g., Fig. 6). Further analysis of the streamwise flux according to the approach suggested by Fairall (1984) suggested that a few large fluxes obtained from the FSSP were erroneous due to wind ramming.

Apparently, neither the eddy correlation nor the wind speed profile system provided a completely accurate value for the Reynolds stress during CACHE-1. The 200-s filter used in the eddy flux data processing presumably removed some "large eddy" momentum transport but had no effect on LW or heat fluxes. This last result implies that small scale turbulence carries nearly all of the LW and heat flux but only a portion of the momentum flux at Cheeka Peak, making any interpretation of momentum-droplet flux relationships problematic.

Slinn (1982) developed a theoretical model which predicted that mean scaled particle (LW here) and momentum fluxes should behave similarly in the absence of significant pressure effects. Measurements performed by Beswick et al. (1991) and Gallagher et al. (1992a, b) suggest that the ratio of LW to momentum deposition velocities is approximately 1.0 except for very low LWC clouds. This approach produced inconclusive results at Cheeka Peak during CACHE-1 in that different events had different ratios of droplet to momentum deposition velocity (Table 1).

The lack of flux proportionality in these data should also be reflected in a comparison of flux cospectra (Wyngaard and Cote, 1972; Hicks and McMillen, 1988). During CACHE-1 there was no cospectral similarity in the LW and momentum fluxes at Cheeka Peak (Fig. 10), presumeably because there are differences between the surface sinks of momentum and droplets. Wind tunnel studies of momentum transport to vegetation (Thom, 1968; Landsberg and Thom, 1971) show that form pressure drag on bluff bodies dominates skin frictional drag. In complex terrain such as upwind of Cheeka Peak, bluff body effects likely are more pronounced than for relatively

homogeneous fetches. The dominant sink for momentum probably is via pressure drag which is proportional to the streamwise-normal area of a given forest element (Thom, 1975) whereas inertial impaction of droplets is most efficient for the small cross-sectional elements of the forest (needles). Thus, the absense of proportionality between droplet and momentum fluxes during CACHE-1 may correctly reflect differences in their sinks. Droplet-vertical velocity cospectra (Fig. 10) are not expected to be affected by the terrain upwind of Cheeka Peak; a hill's effect is limited to suppression of energy in the large eddies (Panofsky et al., 1982). In contrast, small scale eddies transport liquid water droplets at Cheeka Peak.

The size dependence of mean scaled LW flux (Fig. 9) suggests that processes other that droplet interception by the forest canopy were important to the turbulent LW flux at Cheeka Peak during CACHE-1. Impaction efficiency for cloud droplets decreases from 50% at 15 μm to 5% for 5 μm diameter droplets (assuming 5 m s^{-1} windspeed, 4 mm as the characteristic fir needle dimension, and impaction efficiencies from Mohnen and Kadlecek, 1988). Thus, in the absence of additional processes, the magnitude of the turbulent LW flux should decrease rapidly towards zero for diameters $< 10\ \mu$m. However, a change in the sign of LW flux cannot be explained by inefficient impaction.

The FSSP inlet ("face") velocity was equal to the mean streamwise windspeed such that isokinetic sampling typically was achieved. Any droplet size dependence in the FSSP aspiration efficiency depends upon the ratio of streamwise, ambient windspeed to the inlet face velocity (U_a/U_f) (Vincent, 1989). Since the FSSP inlet was isokinetic relative to the mean windspeed, no overall bias is expected in CACHE-1 values for droplet number concentration. Of particular interest is whether instantaneous departures from isokinetic sampling should result in any size-dependence in LW flux or deposition velocity. Near the atmosphere-forest boundary, downdrafts have larger streamwise wind velocities than do updrafts (i.e., momentum flux exists; Stull, 1988) but the FSSP face velocity is constant. Thus, the potential exists for the FSSP to produce size-dependent fluxes because U_a/U_f is different for updrafts and downdrafts.

Specification of the appropriate face velocity for the droplets that actually pass through the FSSP sensing area requires velocity traverses and inlet flow modeling; such analyses are beyond the scope of the present investigation and have not been performed elsewhere (D. Baumgardner, personal communication). Instead, we calculated the streamwise, ambient 30 min mean wind velocity separately for updrafts and downdrafts and compared their ratio ($R_1 = U_{a,w>0}/U_{a,w<0}$) to the measured size dependence in droplet deposition velocity. If the upward LW fluxes derived from the effect of momentum flux on FSSP aspiration efficiency, periods with $R_1 \sim 1$ would not have upward fluxes for small cloud droplets but periods with $R_1 \ll 1$ would. The CACHE-1 data display no change in the size dependence of droplet deposition velocity with variation in R_1, suggesting that the results are insensitive to the FSSP aspiration efficiency for observed conditions ($0.93 < R_1 < 0.99$). The upward LW fluxes for small cloud droplets (dia $\leqslant 8\ \mu$m) must result from either a LWC source located below the 10 m measurement location or from phase change processes.

Since eddy correlation quantifies net fluxes, results are similar for a droplet sink above and a source below the measurement height; both lead to an upward net flux of the affected cloud droplets. For example, an upward LW flux would result from cloudtop entrainment of "dry" air and subsequent droplet evaporation in downdrafts. The resulting deficit of droplets in downward moving air ($w' < 0$) from evaporation is indistinguishable from an excess of droplets in updrafts ($w' > 0$) due to a canopy source. These effects could subtract from the downward LW flux associated with droplet interception and impaction onto the forest canopy. A consideration of the processes themselves, especially the resulting time- and size-dependence in LW flux, can help identify the factors influencing upward small droplet fluxes at Cheeka Peak.

The forest canopy is a potential source of small droplets or aerosol. Splash droplets as small as 5 μm result from the impaction of a 5 mm dia raindrop onto a leaf (Fitt et al., 1982; Gregory et al., 1959). Detrainment of pollen and spores during rainfall injects particles into the atmosphere with aerodynamic diameters of 8 μm at concentrations $\sim 10^2$ m^{-3} (Aylor and Sutton, 1992). This pathway cannot account for observed upward fluxes of small cloud droplets (dia $\leqslant 8\ \mu$m) present

at concentrations of $\geqslant 10^7\ m^{-3}$ (Fig. 8) during non-precipitating cloud.

The observed upward flux of small droplets likely was the result of one or several phase change processes. Eddy correlation measurements quantify turbulent fluxes; fluxes associated with the mean flow are removed in the covariance calculation (eq. (1)). Candidate phase change processes include incremental droplet nucleation and condensational growth due to expansional cooling associated with turbulent updrafts, evaporation in turbulent downdrafts due to cloudtop entrainment and adiabatic compressional warming, and evaporation in updrafts related to daytime surface heating.

Phase change effects are detectible in different ways in the eddy correlation fluxes. For example, the end products of complete droplet evaporation would not be observed because the FSSP rarely detects aerosol (most are too small). Water continuity with phase change cannot be tracked because in-cloud water vapor measurements were not available. Partial droplet evaporation represents a sink for some droplets and a source of smaller droplets (observed here when the final diameter is greater than $2\,\mu m$). Phase change processes affect the eddy correlation results only when they occur over time scales that are shorter than or equal to those for droplet turbulent transport.

The aerosol chemical composition at Cheeka Peak under conditions of marine flow is dominated by hygroscopic compounds such as submicrometer (dia $< 1\,\mu m$) ammonium bisulfate and supermicrometer sodium chloride with few or no hygrophobic components (Covert, 1988). These aerosol, when exposed to supersaturated conditions, quickly form cloud droplets. Nucleation of most of these CCN produces droplets typically $0.2\,\mu m$ diameter at the time of activation (Rogers and Yau, 1989) with a smaller number of up to $6\,\mu m$ droplets forming on supermicrometer seasalt CCN. Thus, nucleation of preexisting marine aerosol in turbulent eddies is consistent with the observed upward turbulent flux of small cloud droplets but most of those droplets require some condensational growth before they would be observed by the FSSP.

Field measurements of CCN spectra at Cheeka Peak suggest a typical peak supersaturation (S) of 0.3% during spring (Ramsey–Bell et al., 1990). Periods with substantial entrainment can produce in-cloud relative humidities (RH) perhaps as low as ~98% (Pruppacher and Klett, 1978). These values for RH and S bound expected time scales for droplet condensation and evaporation at Cheeka Peak. Since subsaturated conditions could occur with larger deviations from saturation than supersaturated conditions, time scales for evaporation can be shorter than those for condensational growth. Since in-cloud RH was unknown during CACHE-1, typical values are chosen to examine evaporation time scales that might apply to the scaled LW fluxes for the "*a*" and "*b*" events during CACHE-1 (Fig. 11).

Evaporation of cloud droplets was characterized as an e-folding-diameter adaptation time (Pruppacher and Klett, 1978) using a numerical model that accounts for vapor diffusion and heat conduction from an internally isothermal droplet, neglecting solute and curvature effects (Anderson, 1992). For an air temperature of 10°C and assumed in-cloud RH of 99.3%, the calculated e-folding evaporation times were 3, 9, 17, and 35 seconds for droplet diameters of 4, 7, 10, and $14\,\mu m$, respectively. For comparison, characteristic time scales for upward (or downward) vertical motion for the typical CACHE-1 eddies which transport LWC are ~10 seconds (Subsection 4.7).

The smallest droplets adjust towards their equilibrium size while the larger droplets are relatively insensitive to saturation status over 10 second turbulent time scales; the maximum diameter of the droplets that will be affected over a limited time period is dependent upon the relative humidity (RH). Here "measureable evaporation" will be used to refer to a decrease in droplet diameter of at least $3\,\mu m$, the width of a FSSP size interval. An eddy arriving at 10 m agl containing cloud droplets in subsaturated air at 99.3% RH would experience measureable evaporation of droplets with diameters $\leqslant 14\,\mu m$. If the RH was 99.7%, only droplets with diameters $\leqslant 10\,\mu m$ would have had time to evaporate prior to further vertical transport in the turbulent wind field. At 98.7% RH, all droplets originally $30\,\mu m$ dia, or smaller, would experience measureable evaporation.

The typical turbulent downdraft spends ~10 seconds descending prior to arrival at the 10 m measurement height such that adiabatic compressional warming results in only small changes in the

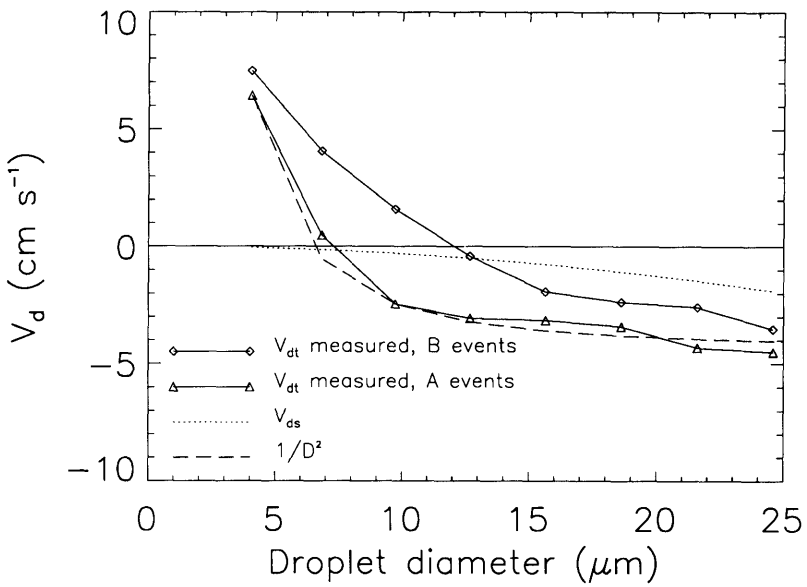

Fig. 11. Average values for mean-scaled liquid water flux (deposition velocity, v_{dt} for the turbulent component; v_{ds} for sedimentation) for both "*a*" and "*b*" events ($a = \sigma_L/\bar{L} < 0.3$ and $b = \sigma_L/\bar{L} > 0.4$) compared to both a $[1/d^2]$ fall-off and to calculated droplet sedimentation velocity.

saturation ratio ($\sigma_w = 60$ cm s^{-1}; T increase is <0.1°C thus S decrease is <0.1%). Adiabatic warming in turbulent eddies represents a minor influence on the vertical distribution of LWC compared to other phase change effects that correlate with turbulent eddy motions.

During daytime, radiative heating can warm surface level air and this process may reduce the saturation ratio in upward moving eddies. The occurrence of near-neutral stability for both "*a*" and "*b*" events as well as the fact that one steady "*a*" event occurred during daytime (25 May) both suggest that surface-driven phase change processes should have had a minimal effect on droplet size during CACHE-1. The remaining candidates for the phase change processes affecting the CACHE-1 events are condensational growth and evaporation associated with cloudtop entrainment, both of which can result in an upward turbulent flux of small cloud droplets.

The size dependence in scaled LW flux during the "*a*" events is consistent with phase change processes in that smaller droplets are affected more than large droplets. This size dependence presumeably reflects the fact that droplets with the same history each gain or lose the same surface area per unit time (Pruppacher and Klett, 1978; Rogers and Yau, 1989) and their relative surface area change is thus $1/d^2$. Fig. 11 demonstrates that a $[1/d^2]$ dependence was observed in the average deposition velocity (a relative change itself) of smaller droplets for "*a*" events.

Comparison of the size dependence of LW flux for "*a*" and "*b*" events suggests that one or more phase change processes were more important during the "*b*" events. The "*b*" events had lower mean LWC, larger $\sigma_L/\bar{L}$, and display an upward v_{dt} that is shifted towards larger diameters. Evaporation is consistent with the differences between the "*a*" and "*b*" events in that it lowers LWC and increases its variability (Baker et al., 1982; Blyth et al., 1980). Evaporation associated with turbulent air motions shifts the deposition velocity curve from that for the steady "*a*" events towards upward fluxes for progressively larger droplets as in-cloud RH decreases ("*b*" cloud events). Evaporation time scales for droplet diameters that correspond to a shift from downward (interception loss at the surface dominates) to upward (evaporation dominates) LW deposition velocities are consistent with an in-cloud RH of 99.7% for the "*a*" cloud events but 99.3% for the "*b*" events.

Further identification of the specific phase

change processes driving the observed upward fluxes of small droplets remains a topic for future research. The sensitivity of the scaled LW flux to the uniformity of droplet histories, pre-cloud conditions (CCN number, temperature, and RH), the extent and type of "dry" air entrainment, and variation in turbulent transport time scales should be evaluated using a cloud parcel model (Jensen et al., 1985). Measurements of below-cloud temperature and RH will allow the determination of an "adiabatic" reference deposition velocity curve that includes the effects of nucleation, condensational growth, and droplet interception but does not include evaporation due to entrainment or surface heating. This "adiabatic" cloud deposition velocity could correspond to the curve for "*a*" events on Fig. 11 but more likely lies to the left of the "*a*" curve, depending upon whether evaporation affected the "*a*" events. Inspection of Fig. 8 for 22 April reveals a bimodal shape, suggesting that evaporation may have influenced LW flux for that particular event.

For variable LWC cloud events, net upward turbulent fluxes of integrated LWC can occur. Analysis of three "*b*" events suggested that, when phase change effects (important for dia $< 13\,\mu$m for "*b*" events) extend to droplets at the volume mean diameter (e.g., the 10 April event; see Table 1), evaporation can be more important than droplet impaction for determining the integrated LW flux. The "*b*" cloud events more nearly reflect typical LWC content (LWC $\leqslant 0.2$ gm/m^3) and integrated LW flux (small in magnitude and variable in direction) at Cheeka Peak during April and May of 1993 than do the "*a*" steady cloud events. It is possible that downward integrated LW fluxes do not occur during periods when "sufficiently" subsaturated cloud interacts with a forest canopy.

Subsequent measurements will help identify the extent to which evaporation processes such as cloudtop entrainment, or possibly surface heating, offset the expected deposition of cloudwater onto the forest canopy. For the present, a lower diameter cutoff for eddy correlation measurements of LW interception is seen to depend on the extent of evaporation; nocturnal cloud represents the preferred conditions for measuring "occult deposition" at Cheeka Peak.

In order to bound the importance of "occult deposition" to hydrological and chemical cycles at Cheeka Peak, one could assume that the total cloud LW deposition rate from the CACHE-1 "*a*" events and spring cloud frequency are representative of annual values (likely overestimating LW turbulent fluxes, given the occurrence of increased evaporation during "*b*" events). Under these assumptions, ~ 12 cm/yr of water is deposited via turbulent transport and impaction. The addition of a smaller sedimentation component produces roughly 20 cm/yr of total cloud liquid water deposited; this is 10% of the water deposited via rain. Since cloudwater has five to ten times higher solute concentrations than rain at Cheeka Peak (Vong and Kowalski, 1994), the upper bound for the total amount of sulfur, nitrogen, and other trace species removed from the atmosphere during cloud immersion is therefore 50% of that deposited via precipitation at this "wet" site. Previously, cloud water chemical deposition had been estimated as equal to or greater than that due to precipitation (Vong et al., 1991; Lovett et al., 1982).

6. Conclusions

A consistent feature of cloud at Cheeka Peak during CACHE-1 is the occurrence of downward integrated LW turbulent fluxes preferentially during periods of low relative LWC variability ($\sigma_L/\bar{L} < 0.3$) and high LWC. Observed turbulent fluxes of cloud droplets were associated with both turbulent transport down the gradient established by the surface impaction sink and phase changes which covary with vertical winds. The precision of the scalar measurements was excellent while the principal uncertainties in the covariances were readily identified and corrected. Agreement between measured droplet deposition velocities and predictions for particle deposition velocities (Slinn, 1982), when taken with small experimental uncertainties, suggests that the observed eddy correlation liquid water fluxes were correctly determined, although they may only be representative of the 10 m agl point of measurement. Conditions of low LWC variability represented the best oportunity to quantify droplet impaction

onto elements of the forest canopy because phase change processes were restricted to droplets with very little liquid water mass. Estimates of chemical deposition via droplet turbulent transfer and impaction onto the canopy surface elements suggest that this process represents $\leqslant 50\%$ of the chemical deposition associated with precipitation at the site.

7. Acknowledgements

This work was supported by National Science Foundation grant #ATM9118316 (Atmospheric Chemistry desk). The authors thank Jeff Shykula and Fred Brechtel for field work and are especially indebted to David Covert and Martin Gallagher for many useful discussions.

REFERENCES

Anderson, T. L. 1992. *Optimization of a counterflow virtual impactor (CVI) for studying aerosol effects on cloud droplet number.* PhD thesis, University of Washington, Seattle, 232 pp., 1992.

Arends, B. G., Kos, G. P. A., Wobrock, W., Schell, D., Noone, K. J., Fuzzi, S. and Pahl, S. 1992. Comparison of techniques for measurements of fog liquid water content. *Tellus* **44B**, 604–611.

Atakturk, S. S. and Katsaros, K. B. 1989. The *K*-gill: a twin propeller-vane anemometer for measurements of atmospheric turbulence. *J. Atmos. Ocean. Tech.* **6**, 509–515.

Aylor, D. E. and Sutton, T. B. 1992. Release of Venturia inaequalis ascospores during unsteady rain: relationship to spore transport and deposition. *Phytopathology* **82**, 532–540.

Baker, M. B., Blyth, A., Carruthers, D., Caughey, S. and Choularton, T. W. 1982. Field studies of the effect of entrainment upon the structure of clouds at Great Dun Fell. *Quart. J. Roy. Meteorol. Soc.* **108**, 899–916.

Baumgardner, D. 1983. An analysis and comparison of five water droplet measuring instruments. *J. Clim. Appl. Meteor.* **22**, 891–910.

Baumgardner, D., Strapp, W. and Dye, J. E. 1985. Evaluation of the forward scattering spectrometer probe. Part II: Corrections for coincidence and dead-time losses. *J. Atmos. Ocean. Tech.* **2**, 626–632.

Beswick, K. M., Hargreaves, K., Gallagher, M. W., Choularton, T. W. and Fowler, D. 1991. Size-resolved measurements of cloud droplet deposition velocity to a forest canopy using an eddy correlation technique. *Quart. J. Roy. Meteorol. Soc.* **117**, 623–645.

Betts, A. K. 1990. Diurnal variation of California coastal stratocumulus from two days of boundary layer soundings. *Tellus* **42A**, 302–304.

Blackman, R. B. and Tukey, J. W. 1958. *The measurement of power spectra.* Dover Publ., NY, USA.

Blaskovic, M., Davies, R. and Snider, J. B. 1991. Diurnal variation of marine stratocumulus over San Nicolas Island during July 1987. *Monthly Weather Review* **119**, 1469–1478.

Blyth, A. M., Choularton, T., Fullerton, G., Latham, J., Mill, C., Smith, M. and Stromberg, I. 1980. The influence of entrainment on the evolution of cloud droplet spectra. *Quart. J. Roy. Meteorol. Soc.* **106**, 821–840.

Choularton, T. W., Consterdine, D., Gardner, I., Gay, B., Hill, M., Latham, J. and Stromberg, I. 1986. Field studies of the optical and microphysical characteristics of clouds enveloping Great Dun Fell. *Quart. J. Roy. Meteorol. Soc.* **112**, 131–148.

Covert, D. S. 1988. North Pacific marine background aerosol: average ammonium to sulfate molar ratio equals 1. *J. Geophys. Res.* **93**, 8455–8458.

Dabberdt, W. F., Lenschow, D., Horst, T., Zimmerman, P., Oncley, S. and Delany, A. C. 1993. Atmosphere-Surface Exchange Measurements. *Science* **260**, 1472–1480.

Dollard, G. J., Unsworth, M. H. and Harvey, M. J. 1983. Pollutant transfer in uplands regions by occult deposition. *Nature* **302**, 341–343.

Duan, B., Fairall, C. W. and Thomson, D. W. 1988. Eddy correlation measurements of the dry deposition of particles in wintertime. *J. Applied Meteorol.* **27**, 642–652.

Fairall, C. W. 1984. Interpretation of eddy correlation measurements of particulate deposition and aerosol flux. *Atmos. Environ.* **18**, 1329–1337.

Fitt, B. D. L., Lysandrou, M. and Turner, R. 1982. Measurement of spore-carrying splash droplets using photographic film and an image-analyzing counter. *Plant Path.* **31**, 19–34.

Gallagher, M. W., Beswick, K. M., Choularton, T. W., Coe, H., Fowler, D. and Hargreaves, K. 1992a. Measurements and modelling of cloudwater deposition to moorland and forests. *Environ. Poll.* **75**, 97–107.

Gallagher, M. W., Beswick, K. M. and Choularton, T. W. 1992b. Measurement and modelling of cloudwater deposition to a snow-covered forest canopy. *Atmos. Environ.* **26A**, 2893–2904.

Gerber, H. 1991. Direct measurement of suspended particulate volume concentration and far infrared extinction coefficient with a laser diffraction instrument. *Applied Optics* **30**, 4824.

Gregory, P. H., Guthrie, E. J. and Bunce, M. E. 1959. Experiments on splash dispersal of fungus spores. *J. Gen. Microbio.* **20**, 328–354.

Hicks, B. B. and McMillen, R. T. 1988. On the measure-

ment of dry deposition using imperfect sensors and in non-ideal terrain. *Bound. Layer Meteorol.* **42**, 79–94.

Hojstrup, J. 1993. A statistical data screening procedure. *Meas. Sci. Technol.* **4**, 153–157.

Jenkins, G. M. and Watt, D. G. 1968. *Spectral analysis and its applications*. Holden-Day, Oakland, CA.

Jensen, J. B., Austin, P. H., Baker, M. B. and Blyth, A. M. 1985. Turbulent mixing, spectral evolution, and dynamics in a warm cumulus cloud. *J. Atmos.* Sci. **42**, 173–192.

Katen, P. C. and Hubbe, J. M. 1985. An evaluation of optical particle counter measurements of the dry deposition of atmospheric aerosols. *J. Geophys. Res.* **90 D1**, 2145–2160.

Landsberg, J. J. and Thom, A. S. 1971. Aerodynamic properties of a plant of complex structure. *Quart. J. Roy. Meteorol. Soc.* **94**, 565–570.

Lee, G., Zhuang, L., Huebert, B. J. and Meyers, T. P. 1993. Concentration gradients and dry deposition of nitric acid vapor at the Mauna Loa Observatory, Hawaii. *J. Geophys. Res.* **98 D7**, 12661–12671.

Lovett, G. M., Reiners, W. A. and Olson, R. K. 1982. Cloud droplet deposition in subalpine balsam fir forests: hydrological and chemical inputs. *Science* **218**, 1303–1304.

Lovett, G. M. 1984. Rates and mechanisms for cloud water deposition to sub-alpine balsam fir forest. *Atmos. Environ.* **18**, 361–371.

Lovett, G. M. and Kinsman, J. D. 1990. Atmospheric pollutant deposition to high-elevation ecosystems. *Atmos. Environ.* **24A**, 2767–2786.

Lumley, J. L. and Panofsky, H. A. 1964. *The structure of atmospheric turbulence*. Wiley and Sons, NY.

McMillen, R. T. 1986. *A BASIC program for eddy correlation in non-simple terrain*. NOAA tech. report ARL-147, NOAA ERL, 32 pp., Silver Spring, MD.

McMillen, R. T. 1988. An eddy correlation technique with extended applicability to non-simple terrain. *Bound. Layer. Meteorol.* **43**, 231–245.

Miller, E. K., Friedland, A., Arons, E., Mohnen, V. A., Battle, J., Panek, J. A., Kadlecek, J. and Johnson, A. H. 1993. Atmospheric deposition to forests along an elevational gradient at Whiteface Mountain, NY, USA. *Atmos. Environ.* **27A**, 2121–2136.

Mohnen, V. A. and Kadlecek, J. A. 1989. Cloud chemistry research at Whiteface Mountain. *Tellus* **41B**, 79–91.

Mueller, S. F. 1991. Estimating cloud water deposition to subalpine spruce-fir forests (1). Modifications to an existing model. *Atmos. Environ.* **25A**, 1093–1104.

Noonkester, V. R. 1984. Droplet spectra observed in marine stratus cloud layers. *J. Atmos. Sci.* **41**, 829–845.

Norment, H. G. 1987. Numerical studies of sampling efficiencies of the ASCME and PMS aspirator hydrometer measurement instruments. *J. Atmos. Ocean. Tech.* **4**, 253–263.

Panofsky, H. A., Larko, D., Lipschutz, R., Stone, G., Bradley, E., Bowen, A. and Hojstrup, J. 1982. Spectra of velocity components over complex terrain. *Quart. J. Roy. Meteorol. Soc.* **108**, 215–230.

Pruppacher, H. R. and Klett, J. D. *Microphysics of clouds and precipitation*. Reidel, Boston, 1978.

Ramsey-Bell, D. C., Anderson, T. L. and Covert, D. S. 1990. Cloud condensation nuclei measurements in the coastal marine boundary layer of the NE Pacific Ocean, paper A11A-07. Presented at *Amer. Geophysical Union Fall Meeting*, San Francisco, CA.

Rogers, R. R. and Yau, M. K. 1989. *A short course in cloud physics*. Pergammon, Oxford.

Slinn, W. G. N. 1982. Predictions for particle deposition to vegetative canopies. *Atmos. Environ.* **16**, 1785–1794.

Stull, R. B. 1988. *An introduction to boundary layer meteorology*, Kluwer, The Netherlands.

Thom, A. S. 1968. The exchange of momentum, mass and heat between an artificial leaf and the airflow in a wind-tunnel. *Quart. J. Roy. Meteorol. Soc.* **94**, 44–55.

Thom, A. S. 1975. Momentum, mass, and heat exchange of plant communities. In: L. L. Monteith (ed.): *Vegetation and the atmosphere*, vol. I. Academic Press, London, pp. 57–109.

Thorne, P. G., Lovett, G. and Reiners, W. A. 1982. Experimental determination of droplet impaction on canopy elements of balsam fir. *J. Applied Meteorol.* **21**, 1413–1416.

Vincent, J. H. 1989. *Aerosol sampling, science and practice*. Wiley and Sons, NY.

Vong, R. J., Sigmon, J. and Mueller, S. F. 1991. Cloudwater deposition to Appalachian mountain forest. *Environ. Sci. Tech.* **25**, 1014–1021.

Vong, R. J., Hansson, H.-C., Ross, H. B., Covert, D. S. and Charlson, R. J. 1988. Northeastern Pacific submicrometer aerosol and rainwater composition: a multivariate analysis. *J. Geophys. Res.* **93 D2**, 1625–1637.

Vong, R. J. and Kowalski, A. S. 1994. Eddy correlation measurements of cloud liquid water and chemical fluxes, abstract #FA6.14. Preprints: *Conference on atmospheric chemistry*. Amer. Meteorol. Soc., Nashville, TN.

Wesley, M. L. 1970. *Eddy correlation measurements in the atmospheric surface layer over agricultural crops*. PhD thesis. Univ. Wisconsin, Madison, WI.

Wesley, M. L. 1983. Turbulent transport of ozone to surfaces common in the eastern half of the United States. In: *Trace atmospheric constituents: properties, transformations and fates*, ed. S. E. Schwartz. Wiley.

Wyngaard, J. C. 1988. The effects of probe-induced flow distortion on atmospheric turbulence measurements: extension to scalars. *J. Atmos.* Sci. **45**, 3400–3412.

Wyngaard, J. C. and Cote, O. R. 1972. Cospectral similarity in the atmospheric surface layer. *Quart. J. Roy. Meteorol. Soc.* **98**, 590–603.